THE JOURNAL OF BIOLOGICAL CHEMISTRY
Vol. 280, No. 35, Issue of September 2, pp. 31220–31229, 2005

Printed in U.S.A.

Crystal Structure of Pyridoxal Kinase in Complex with Roscovitine and Derivatives*

Received for publication, January 21, 2005, and in revised form, June 24, 2005
Published, JBC Papers in Press, June 28, 2005, DOI 10.1074/jbc.M500805200

Lin Tang‡§, Ming-Hui Li‡, Peng Cao‡§, Feng Wang‡§, Wen-Rui Chang‡, Stéphane Bach¶, Jens Reinhardt¶, Yoan Ferandin¶, Hervé Galons‖, Yongqin Wan, Nathanael Gray**, Laurent Meijer¶, Tao Jiang‡ ‡‡, and Dong-Cai Liang‡**

*From the ‡National Laboratory of Biomacromolecules, Institute of Biophysics, Chinese Academy of Sciences, 15 Datun Road, Chaoyang District, Beijing 100101, China, ¶C.N.R.S., Cell Cycle Group, UPS 2682 & UMR 7150 "Mer & Santé," Station Biologique, B.P. 74, 29682 Roscoff cedex, Bretagne, France, the ‖Laboratoire de Chimie Organique 2, Université René Descartes, 4 avenue de l'Observatoire, 75270 Paris cedex 06, France, the **Genomics Institute of the Novartis Research Foundation, Department of Chemistry, San Diego, California 92121, and the §Graduate School of the Chinese Academy of Sciences, Yuquan Road 19A, Beijing 100039, China*

Pyridoxal kinase (PDXK) catalyzes the phosphorylation of pyridoxal, pyridoxamine, and pyridoxine in the presence of ATP and Zn^{2+}. This constitutes an essential step in the synthesis of pyridoxal 5′-phosphate (PLP), the active form of vitamin B_6, a cofactor for over 140 enzymes. (*R*)-Roscovitine (CYC202, Seliciclib) is a relatively selective inhibitor of cyclin-dependent kinases (CDKs), currently evaluated for the treatment of cancers, neurodegenerative disorders, renal diseases, and several viral infections. Affinity chromatography investigations have shown that (*R*)-roscovitine also interacts with PDXK. To understand this interaction, we determined the crystal structure of PDXK in complex with (*R*)-roscovitine, N^6-methyl-(*R*)-roscovitine, and O^6-(*R*)-roscovitine, the two latter derivatives being designed to bind to PDXK but not to CDKs. Structural analysis revealed that these three roscovitines bind similarly in the pyridoxal-binding site of PDXK rather than in the anticipated ATP-binding site. The pyridoxal pocket has thus an unexpected ability to accommodate molecules different from and larger than pyridoxal. This work provides detailed structural information on the interactions between PDXK and roscovitine and analogs. It could also aid in the design of roscovitine derivatives displaying strict selectivity for either PDXK or CDKs.

Pyridoxal kinase (PDXK)[1] catalyzes the phosphorylation of the three forms of vitamin B_6 (pyridoxal, pyridoxamine, and pyridoxine) in the presence of ATP and Zn^{2+}. This phosphorylation constitutes an essential step in the synthesis of pyridoxal 5′-phosphate (PLP), the intracellular active form of vitamin B_6, a key cofactor for at least 140 enzymes, such as aminotransferases and decarboxylases (1–3). PDXK is connected to nervous system functions, because many neurotransmitters such as dopamine, norepinephrine, serotonin, and γ-aminobutyric acid are synthesized by PLP-dependent enzymes (4). The mechanisms underlying pyridoxal kinase inhibition by several drugs have been studied (5). Recently, the crystal structure of PdxY, a PDXK homology protein of *Escherichia coli* was reported (6). Concurrently, the three-dimensional structures of sheep brain PDXK alone and in complex with various ligands (PDXK/ATP, PDXK/AMP-PCP/pyridoxamine, PDXK/ADP/PLP, and PDXK/ADP) have been determined, providing a better understanding of the catalysis mechanism of PDXK (7, 8).

Cyclin-dependent kinases (CDKs) play an important role in the regulation of cell division, apoptosis, transcription, neuronal functions, and exocytosis. The frequent deregulation of CDKs and their regulators in human tumors (9–13) and the involvement of CDK5 in Alzheimer (14), Parkinson (15), Nieman-Pick diseases (16), and ischemia (17) have stimulated an active search for chemical CDK inhibitors (12, 18, 19). Among the numerous inhibitors that have been identified, roscovitine, one of the early compounds, appears to be relatively potent and selective. Because of its cell growth inhibiting and neuroprotective activities, this purine is currently considered as a potential drug to treat, respectively, cancers, glomerulonephritis, and various neurodegenerative diseases (20). Roscovitine exists as two stereoisomers, (*R*)-roscovitine and (*S*)-roscovitine, the (*R*)-roscovitine isomer being slightly more active on CDKs (21–23). (*R*)-Roscovitine has been selected, under the name CYC202 (or Seliciclib), for preclinical and clinical evaluations (24, 25). (*R*)-Roscovitine has been crystallized with two protein kinases, CDK2 (21) and CDK5 (26). Like most CDK inhibitors it binds to the catalytic site of the kinases and acts as a competitive inhibitor for ATP binding (21, 27).

The selectivity of pharmacological inhibitors of protein kinases is an important issue. Because many inhibitors act by interacting within the ATP-binding pocket of their target kinases, a most conserved domain among the 518+ human kinases, concern about their selectivity is sensible. In the accompanying article (32), we showed that (*R*)-roscovitine is a relatively selective CDK inhibitor, based on a selectivity study involving 148 kinases (23). This good selectivity was recently confirmed by a new *in vitro* kinase/ligand competition assay (28). However, affinity chromatography on immobilized (*R*)-

* This work was supported by the National Natural Science Foundation of China Grant 30100026, Chinese Academy of Sciences Grants KSCX1-SW-17 and KJCX2-SW-N06, MOST of China Grants 863-2002BA711A13 and 973-2004CB520801 (to T. J., and D. L.), grants from the Ministère de la Recherche/INSERM/CNRS "Molécules et Cibles Thérapeutiques" Program (to L. M.), EEC Grant FP6–2002 from the Life Sciences & Health, PRO-KINASE Research Project (to L. M.), and the Canceropole Grand-Ouest. The costs of publication of this article were defrayed in part by the payment of page charges. This article must therefore be hereby marked "*advertisement*" in accordance with 18 U.S.C. Section 1734 solely to indicate this fact.

The atomic coordinates and structure factors (codes 1YGK, 1YGJ, and 1YHJ) have been deposited in the Protein Data Bank, Research Collaboratory for Structural Bioinformatics, Rutgers University, New Brunswick, NJ (http://www.rcsb.org/).

‡‡ To whom correspondence should be addressed. Tel.: 86-10-64888510; Fax: 86-10-64888510; E-mail: x-ray@sun5.ibp.ac.cn.

[1] The abbreviations used are: PDXK, pyridoxal kinase; AMP-PCP, adenosine 5′-(β,γ-methylenetriphosphate); CDK, cyclin-dependent kinase; Me_2SO, dimethyl sulfoxide; PLP, pyridoxal 5′-phosphate; Mops, 4-morpholinepropanesulfonic acid; HPLC, high performance liquid chromatography.

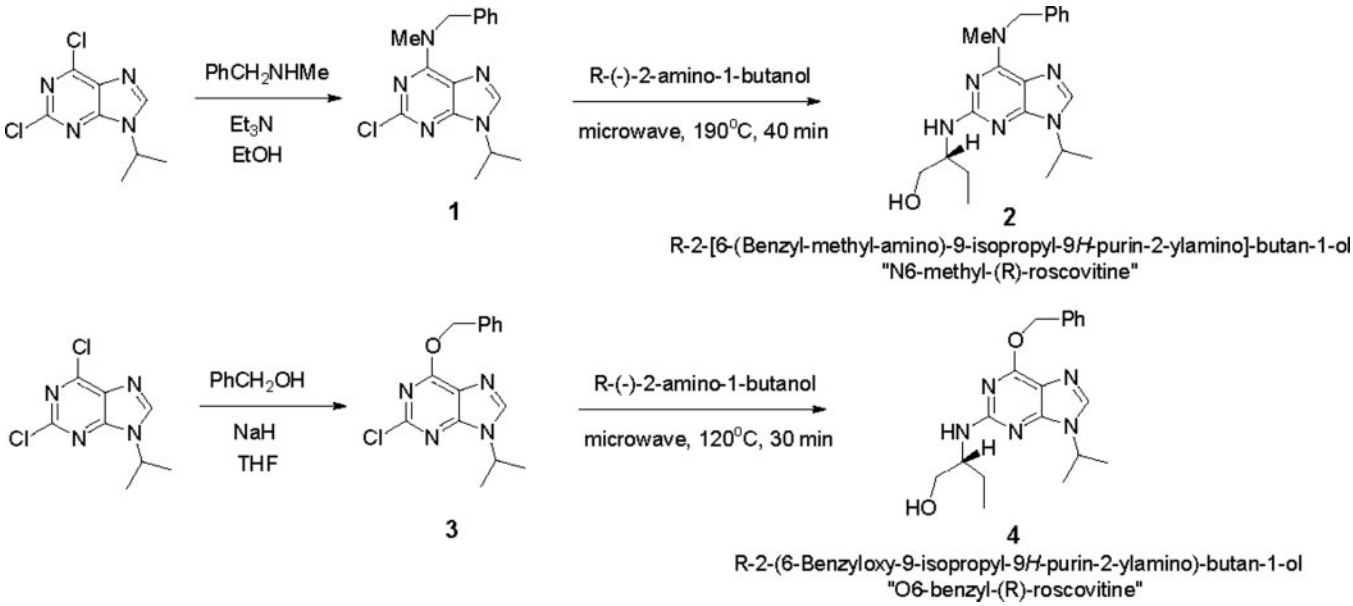

SCHEME 1. **Synthesis of N^6-methyl-(*R*)-roscovitine (2) and O^6-(*R*)-roscovitine (4).**

roscovitine revealed that (*R*)-roscovitine interacts with PDXK from various biological sources (23). In addition, this study showed that ATP competes with the binding of ERK1, ERK2, CDK5, and PDXK to roscovitine, whereas pyridoxal only competes with the binding of PDXK, but not of the protein kinases.

In this study we have solved the crystal structure of PDXK in complex with (*R*)-roscovitine and with two roscovitine derivatives designed not to interact with CDKs. All three purines were found to bind at the pyridoxal-binding site of PDXK, rather than at the expected ATP-binding site. Analysis of the PDXK/roscovitine crystal structure will allow the design of derivatives exclusively interacting with either CDKs or PDXK, thereby leading to new generations of roscovitine-derived pharmacological inhibitors of potential therapeutic interest.

EXPERIMENTAL PROCEDURES

Synthesis of Roscovitine, Roscovitine Derivatives, and Resins Thereof

NMR spectra were recorded on a Bruker 400 MHz spectrometer. Structural assignments were achieved by one- and two-dimensional methods.

(R)- and (S)-Roscovitine

Roscovitine enantiomers were prepared according to Wang *et al.* (22) by a slightly modified procedure. Briefly, to a solution of benzyl-(2-chloro-9-isopropyl-9*H*-purin-6-yl)-methyl-amine (**1**) (1.2 g, 4 mmol) in 5 ml of dimethyl sulfoxide (Me_2SO) was added (*R*)-(−)-2-amino-1-butanol or (*S*)-(+)-2-amino-1-butanol (1 ml, 5 mmol). The mixture was stirred 3 h at 120 °C. After cooling to room temperature, the solution was diluted with water (150 ml) and extracted with CH_2Cl_2 (3 × 50 ml). The organic layer was washed twice with brine, dried over $MgSO_4$, and evaporated. The residue was chromatographed on silica gel using (CH_2Cl_2/ethanol/NEt_3, 95:4.5:0.5) as eluent to afford (*R*)- and (*S*)-roscovitine in 70–76% yield.

(R)-Roscovitine—For (*R*)-roscovitine we used m.p. 104–107 °C. The spectra used was ^{1}H NMR ($CDCl_3$), δ 1.04 (t, 3H, *J* = 7.5 Hz), 1.50 (dd, 6H), 1.60 (m, 2*H*), 3.60 (m, 1*H*), 3.80 (m, 1*H*), 4.60 (septet, 1*H*, *J* = 7.5 Hz), 4.80 (2*H*, s), 4.95(broad s, 1*H*), 5.10(s, 1*H*), 6.05 (s, 1*H*), 7.25 (m, 5*H*), 7.45 (s, 1*H*).

(S)-Roscovitine—For (*S*)-roscovitine we used m.p. 103–106 °C. ^{1}H NMR spectra was identical to the ^{1}H NMR spectra of (*R*)-roscovitine.

R-2-[6-(Benzyl-methyl-amino)-9-isopropyl-9H-purin-2-ylamino]-butan-1-ol ("N^6-methyl-(R)-roscovitine") (2)

A solution of 2,6-dichloro-9-isopropyl-9H-purine (50 mg, 0.22 mmol), *N*-benzylmethylamine (26 mg, 0.22 mmol), and triethylamine (44 mg, 0.43 mmol) in ethanol was stirred at 60 °C for 1 h. The solvent was removed under vacuum, and the residue was purified by HPLC (C_{18} column, eluted with CH_3CN/H_2O with 0.05% trifluoroacetic acid) to afford benzyl-(2-chloro-9-isopropyl-9*H*-purin-6-yl)-methyl-amine (**1**) as a white solid (64 mg, 94%). The spectra used was ^{1}H NMR (methanol-d_4), δ 1.58 (d, 6*H*, *J* = 7.2 Hz), 3.40 (b, 3*H*), 4.79 (septet, 1*H*, *J* = 7.2 Hz), 5.40 (b, 2*H*), 7.24–7.34 (m, 5*H*), 8.11 (s, 1*H*); *m/z* [M^+ + 1] 316.1. A solution of benzyl-(2-chloro-9-isopropyl-9*H*-purin-6-yl)-methyl-amine (**1**) (25 mg, 0.079 mmol) in (*R*)-(−)-2-amino-1-butanol (1.5 ml) in a Smith Process vial was sealed and heated at 190 °C for 40 min using microwave irradiation. Water (15 ml) was then added to the mixture and it was extracted with ethyl acetate (3 × 10 ml). The organic layers were combined, washed with brine (10 ml), and dried with Na_2SO_4. The drying agent was removed and the solvent was evaporated. The resulting residue was purified by HPLC (C_{18} column, eluted with CH_3CN/H_2O with 0.05% trifluoroacetic acid) to afford the title compound as a hygroscopic white solid (31 mg, 80%). The following spectra was used: ^{1}H NMR (methanol-d_4), δ 0.99 (t, 3*H*, *J* = 7.2 Hz), 1.59 (d, 6*H*, *J* = 7.2 Hz), 1.60–1.66 (m, 1*H*), 1.68–1.76 (m, 1*H*), 3.38 (b, 3 H), 3.65–3.71 (m, 2*H*), 3.98–4.06 (m, 1*H*), 4.65–4.75 (m, 1 H), 5.50 (b, 2*H*), 7.28–7.39 (m, 5*H*), 8.03 (s, 1 H); *m/z* [M^+ + 1] 369.2.

R-2-(6-Benzyloxy-9-isopropyl-9H-purin-2-yl-amino)-butan-1-ol

"O^6-Benzyl-(R)-roscovitine" (4)—To a solution of benzyl alcohol (0.11 g, 1.0 mmol) in anhydrous tetrahydrofuran (10 ml) at 0 °C, NaH was added (60% dispersion in mineral oil, 72 mg). It was stirred at this temperature for half an hour and then slowly added into a solution of 2,6-dichloro-9-isopropyl-9*H*-purine (0.20 g, 0.88 mmol) in tetrahydrofuran (10 ml) at 0 °C. The reaction was stirred for 1 h and quenched with saturated NH_4Cl (15 ml). It was extracted with ethyl acetate (3 × 10 ml). The organic layers were combined, washed with brine (10 ml), and dried with Na_2SO_4. The drying agent was then removed, and the solvent was evaporated. The residue was purified by flash column chromatography (silica gel, eluted with EtOAc-hexanes) to afford 6-benzyloxy-2-chloro-9-isopropyl-9*H*-purine (**3**) (0.20 g, 76%). The spectra was ^{1}H NMR (methanol-d_4), δ 1.62 (d, 6*H*, *J* = 6.8 Hz), 4.86 (septet, 1*H*, *J* = 7.2 Hz), 5.64 (s, 2*H*), 7.34–7.41 (m, 3*H*), 7.55 (d, 2*H*, *J* = 6.8 Hz), 8.39 (s, 1*H*); *m/z* [M^+ + 1] 303.1. A solution of 6-benzyloxy-2-chloro-9-isopropyl-9*H*-purine (**3**) (0.10 g, 0.33 mmol) in (*R*)-(−)-2-amino-1-butanol (1.5 ml) in a Smith Process vial was sealed and heated at 120 °C for 30 min using microwave irradiation. Water (15 ml) was then added to the mixture and it was extracted with ethyl acetate (3 × 10 ml). The organic layers were combined, washed with brine (10 ml), and dried with Na_2SO_4. The drying agent was removed, and the solvent was evaporated. The resulting residue was first purified by flash column chromatography (silica gel, eluted with EtOAc-hexanes) and followed by HPLC (C_{18} column, eluted with CH_3CN/H_2O with 0.05% trifluoroacetic acid) to afford the title compound as a hygroscopic white solid (23.4 mg, 15%). The spectra was ^{1}H NMR (methanol-d_4), δ 0.99 (t, 3 H, *J* = 7.2 Hz), 1.53–1.61 (m, 1*H*), 1.63 (d, 6*H*, *J* = 7.2 Hz), 1.74–1.80 (m, 1*H*), 3.59–3.69 (m, 2*H*), 4.00–4.08 (m, 1*H*), 4.85 (septet, 1*H*, *J* = 7.2 Hz), 5.60 (s,

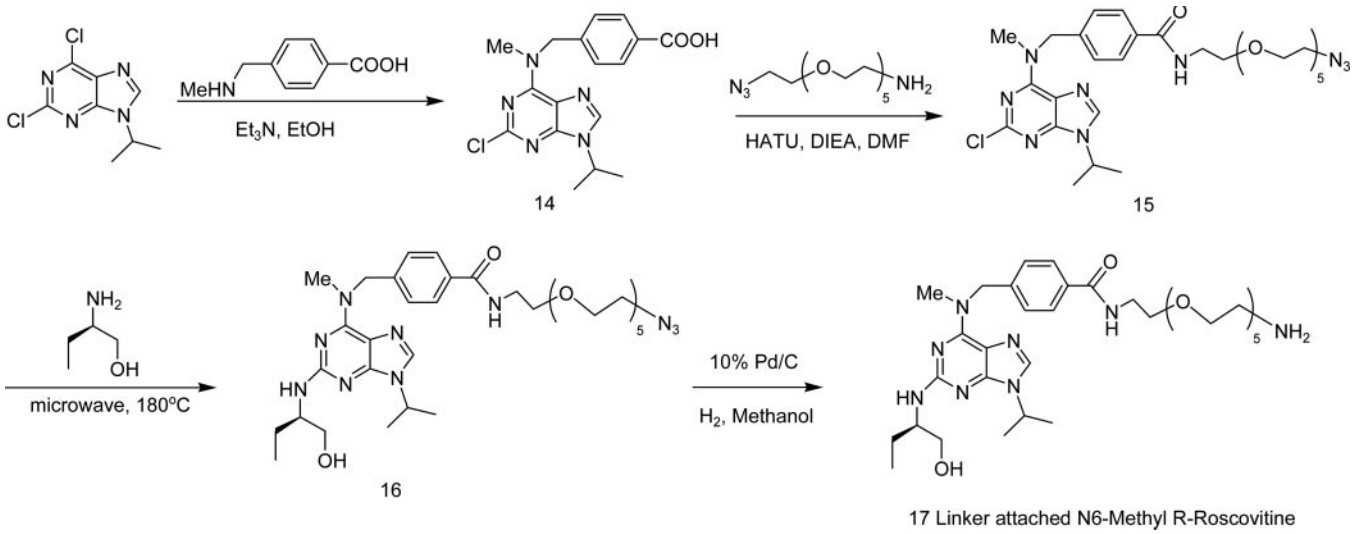

SCHEME 2. **Synthesis of N^6-methyl-(*R*)-roscovitine resin.**

2*H*), 7.32–7.41 (m, 3*H*), 7.52 (d, 2*H*, *J* = 6.8 Hz), 8.82 (s, 1*H*); *m/z* [M$^+$ + 1] 356.2 (Scheme 1).

Purine-agarose Matrices

The (*R*)-roscovitine matrix was prepared as described in the accompanying article (23). Purvalanol (NG-97) matrix was synthesized as previously described (29–31) (Scheme 2).

Synthesis of Linker-attached N^6-methyl-(R)-roscovitine

*4-{[(2-Chloro-9-isopropyl-9H-purin-6-yl)-methylamino]-methyl}-benzoic Acid (**14**)*

A solution of 2,6-dichloro-9-isopropyl-9H-purine (0.45 g, 1.9 mmol), 4-methylaminomethyl-benzoic acid (0.30 g, 1.8 mmol), and triethylamine (0.5 g, 5.0 mmol) in ethanol was stirred at 60 °C for 1 h. The solvent was removed under vacuum, and the residue was purified by column chromatography (silica gel, eluted with ethyl acetate with 10% methanol) to afford benzyl-(2-chloro-9-isopropyl-9*H*-purin-6-yl)-methylamine (14) as a white solid (0.66 mg, 94%); *m/z* [M$^+$ + 1] 360.1.

Azide 15

To a solution of 44-{[(2-chloro-9-isopropyl-9*H*-purin-6-yl)-methylamino]-methyl}-benzoic acid (**14**) (0.18 g, 0.51 mmol) in *N*,*N*-dimethylformamide (4 ml) was added *N*-ethyldiisopropylamine (0.18 ml, 1.0 mmol), 2-[2-(2-{2-[2-(2-azido-ethoxy)-ethoxy]-ethoxy}-ethoxy)-ethoxy]-ethylamine (**3**) (0.23 g, 0.77 mmol), and *O*-(7-azabenzotriazol-1-yl)-*N*,*N*,*N*′,*N*′-tetramethyluronium hexafluorophosphate (0.2 g, 0.51 mmol). The reaction mixture was stirred at room temperature for 3 h and concentrated *in vacuo*. The reaction was concentrated in vacuum and the resulting residue was purified by HPLC (C_{18} column, eluted with CH_3CN/H_2O with 0.035% trifluoroacetic acid) to afford the title compound as a colorless oil (0.22 g, 65%). The spectra was ^{1}H NMR (methanol-d_4), δ 1.56 (d, 6*H*, J = 6.8 Hz), 3.24–3.36 (m, 5*H*), 3.50–3.65 (m, 24*H*), 4.77 (septet, 1*H*, J = 6.8 Hz), 7.38 (d, 2*H*, J = 7.6 Hz), 7.79 (d, 2*H*, J = 7.6 Hz), 8.08 (s, 1*H*); *m/z* [M$^+$ + 1] 647.3.

*Linker-attached N^6-methyl-(R)-roscovitine Azide (**16**)*

A mixture of (**15**) (90 mg, 0.14 mmol) in (*R*)-(−)-2-amino-1-butanol (1.5 ml) in a sealed Smith Process vial was heated at 180 °C for 30 min using microwave irradiation. The reaction mixture was diluted with water (10 ml) and extracted with ethyl acetate (3 × 10 ml). The organic layers were combined and dried with Na_2SO_4. The drying agent was removed and the solvent was evaporated. The resulting residue was purified by HPLC (C_{18} column, eluted with CH_3CN/H_2O with 0.035% trifluoroacetic acid) to afford the title compound as colorless oil (50 mg, 51%). The spectra was ^{1}H NMR (Me_2SO-d_4), δ 0.82–0.92 (m, 3*H*), 1.45–1.50 (m, 7*H*), 1.58–1.64 (m, 1*H*), 3.36–3.60 (m, 31*H*), 3.80–3.88 (m, 1*H*), 4.50–4.62 (m, 1*H*), 7.37 (d, 2*H*, J = 6.8 Hz), 7.81 (d, 2*H*, J = 6.8 Hz), 8.10 (s, 1*H*), 8.45–8.50 (m, 2*H*); *m/z* [M$^+$ + 1] 701.1.

*Linker-attached N^6-methyl-(R)-roscovitine (**17**)*

To a solution of linker-attached N^6-methyl-(*R*)-roscovitine azide (**16**) (70 mg, 0.10 mmol) in methanol (5 ml) was added Pd/C (10%, 50 mg). It was stirred at room temperature under hydrogen atmosphere for 10 min, and the catalyst was removed by filtration. Methanol was removed in vacuum to afford a colorless oil. It was further purified by HPLC (C_{18} column, eluted with CH_3CN/H_2O with 0.035% trifluoroacetic acid) to afford the title compound as a colorless oil (62 mg, 92%). The spectra was ^{1}H NMR (Me_2SO-d_6), δ 0.84–0.89 (m, 3*H*), 1.45–1.50 (m, 7*H*), 1.59–1.62 (m, 1*H*), 2.95–3.00 (m, 2*H*), 3.40–3.60 (m, 29*H*), 3.78–3.85 (m, 1*H*), 4.55–4.61 (m, 1*H*), 7.35 (d, 2*H*, J = 8.0 Hz), 7.73 (b, 3*H*), 7.79 (d, 2*H*, J = 8.0 Hz), 7.91 (s, 1*H*), 8.45 (s, 1*H*); *m/z* [M$^+$ + 1] 675.1.

Affinity Chromatography on Immobilized Roscovitine

Buffers

Homogenization Buffer—The homogenization buffer was 60 mM β-glycerophosphate, 15 mM *p*-nitrophenyl phosphate, 25 mM Mops (pH 7.2), 15 mM EGTA, 15 mM $MgCl_2$, 1 mM dithiothreitol, 1 mM sodium vanadate, 1 mM NaF, 1 mM phenylphosphate, 10 μg of leupeptin/ml, 10 μg aprotinin/ml, 10 μg soybean trypsin inhibitor/ml, and 100 μM benzamidine.

Bead Buffer—The bead buffer was 50 mM Tris (pH 7.4), 5 mM NaF, 250 mM NaCl, 5 mM EDTA, 5 mM EGTA, 0.1% Nonidet P-40, 10 μg/ml leupeptin, aprotinin, and soybean trypsin inhibitor, and 100 μM benzamidine.

Preparation of Extracts

Pork brains were obtained from a local slaughterhouse and directly homogenized and processed for affinity chromatography or stored at −80 °C prior to use. Tissues were weighed, homogenized, and sonicated in homogenization buffer (2 ml/g of material). Homogenates were centrifuged for 10 min at 14,000 × *g* at 4 °C. The supernatant was recovered, assayed for protein content (Bio-Rad protein assay), and immediately loaded batchwise on the affinity matrix.

Affinity Chromatography of Roscovitine Interacting Proteins

Just before use, 10 μl of packed roscovitine beads were washed with 1 ml of bead buffer and resuspended in 600 μl of this buffer. The tissue extract supernatant (3 mg of total protein) was then added; the tubes were rotated at 4 °C for 30 min. After a brief spin at 10,000 × *g* and removal of the supernatant, the beads were washed 4 times with bead buffer before addition of 60 μl of 2× Laemmli sample buffer. Following heat denaturation for 3 min, the bound proteins were analyzed by SDS-PAGE and Western blotting or silver staining as described below.

Electrophoresis and Western Blotting

Antibodies

Some antibodies were obtained from commercial sources: anti-CDK5 C-8 (Santa Cruz, Sc-173, 1:500, 1 h), anti-ERK1/2 (Sigma, M7927, 1:4000, 1 h). Anti-PDXK was generated by Eurogentec Europe (Double XP program). Two rabbits were immunized with a mixture of two human PDXK internal peptides: LLAWTHKHPNNLK (amino acids 241–253) and LRMVQSKRDIEDPEI (amino acids 291–305). The resulting antiserum (1:500, 1 h) cross-reacts with PDXK from a variety of species including mouse, rat, porcine, monkey, and human.

Following heat denaturation for 3 min, the proteins bound to the

roscovitine matrix were separated by 10% SDS-PAGE (0.7 mm thick gels) followed by immunoblotting analysis or silver staining using an Amersham SDS-PAGE silver staining kit. For immunoblotting, proteins were transferred to 0.45-μm nitrocellulose filters (Schleicher and Schuell). These were blocked with 5% low fat milk in Tris-buffered saline/Tween 20, incubated for 1 h with antibodies, and analyzed by Enhanced Chemiluminescence (ECL, Amersham Biosciences).

Protein Kinase Assays

Buffers

Homogenization Buffer—Homogenization buffer was 60 mM β-glycerophosphate, 15 mM *p*-nitrophenyl phosphate, 25 mM Mops (pH 7.2), 15 mM EGTA, 15 mM $MgCl_2$, 1 mM dithiothreitol, 1 mM sodium vanadate, 1 mM NaF, 1 mM phenylphosphate, 10 μg of leupeptin/ml, 10 μg aprotinin/ml, 10 μg of soybean trypsin inhibitor/ml, and 100 μM benzamidine.

Buffer C—Homogenization buffer but 5 mM EGTA, no NaF, and no protease inhibitors.

Kinase Preparations and Assays

Kinase activities were assayed in buffer C, at 30 °C, at a final ATP concentration of 15 μM. Blank values were subtracted and activities were calculated as picomoles of phosphate incorporated during a 10-min incubation. The activities were expressed in % of the maximal activity, *i.e.* in the absence of inhibitors. Controls were performed with appropriate dilutions of dimethyl sulfoxide. Unless otherwise stated, the P81 phosphocellulose assay was used.

CDK1/Cyclin B—CDK1/cyclin B was extracted in homogenization buffer from M phase starfish (*Marthasterias glacialis*) oocytes and purified by affinity chromatography on p9CKShs1-Sepharose beads, from which it was eluted by free p9CKShs1 as previously described (27). The kinase activity was assayed in buffer C, with 1 mg of histone H1/ml, in the presence of 15 μM [γ-^{33}P]ATP (3,000 Ci/mmol; 10 mCi/ml) in a final volume of 30 μl. After a 30-min incubation at 30 °C, 25-μl aliquots of supernatant were spotted onto 2.5 × 3-cm pieces of Whatman P81 phosphocellulose paper, and 20 s later, the filters were washed five times (for at least 5 min each time) in a solution of 10 ml of phosphoric acid/liter of water. The wet filters were counted in the presence of 1 ml of ACS (Amersham Biosciences) scintillation fluid.

CDK2/Cyclin E—CDK2/cyclin E was obtained from insect cell lysates, purified on p9CKShs1-Sepharose, and assayed as described for CDK1/cyclin B.

CDK5/p25—CDK5/p25 was reconstituted by mixing equal amounts of recombinant mammalian CDK5 and p25 expressed in *E. coli* as glutathione *S*-transferase fusion proteins and purified by affinity chromatography on glutathione-agarose (vectors kindly provided by Dr. J. H. Wang) (p25 is a truncated version of p35, the 35-kDa CDK5 activator). Its activity was assayed with histone H1 in buffer C as described for CDK1/cyclin B.

CK1—Native CK1 was purified from rat liver and assayed in buffer C, with casein, in the presence of 15 μM [γ-^{33}P]ATP (3000 Ci/mmol; 10 mCi/ml) in a final volume of 30 μl. After a 30-min incubation at 30 °C, 25-μl aliquots of supernatant were loaded on 3MM filters and extensively washed with 10% trichloroacetic acid, before counting.

DYRK1A—DYRK1A was expressed as a glutathione *S*-transferase fusion protein in *E. coli* (vector kindly provided by Dr. W. Becker, Institute for Pharmacology and Toxicology, Aachen, Germany) and purified by affinity chromatography on glutathione-agarose. Its kinase activity was assayed in buffer C, with 0.16 mg of myelin basic protein/ml, in the presence of 15 μM [γ-^{33}P]ATP (3000 Ci/mmol; 10 mCi/ml) in a final volume of 30 μl. After 30 min incubation at 30 °C, 25-μl aliquots of supernatant were treated as described above.

ERK2—ERK2 was obtained as a His-tagged recombinant enzyme and activated by recombinant mitogen-actived protein kinase kinase. It was assayed as described above for CDK1/cyclin B.

Pyridoxal Kinase Crystallization

Pyridoxal kinase was isolated and purified from sheep brain as described previously (1). Crystals of PDXK in complex with roscovitine and its derivatives were obtained by co-crystallization under conditions similar to those used for the PDXK/AMP-PCP/pyridoxamine crystallization (8). For the PDXK·(*R*)-roscovitine and PDXK·N^6-methyl-(*R*)-roscovitine complexes, a protein solution was prepared containing 10 mg/ml PDXK and 3 mM roscovitine in 50 mM KH_2PO_4/K_2HPO_4 (pH 8.2). Crystals of PDXK complexes with these two purines were grown using the hanging drop vapor diffusion technique with a reservoir solution of 1.4 M ammonium sulfate and 100 mM KH_2PO_4/K_2HPO_4 (pH 8.2), in a drop obtained by mixing 1 μl of protein solution and 1 μl of reservoir solution. Crystals appeared after about 1 month at a constant 17 °C. Similar conditions were used for the crystallization of the PDXK·O^6-(*R*)-roscovitine complex, except that pH was 6.4.

Structure Determination and Refinement

X-ray diffraction data for PDXK/(*R*)-roscovitine co-crystals were collected using a Mar345 image plate in the Synchrotron Radiation Laboratory, Institute of High Energy Physics (Beijing, China). Data for PDXK/O^6-(*R*)-roscovitine and PDXK/N^6-methyl-(*R*)-roscovitine crystals were collected using a Rigaku R-Axis-IP IV++ imaging plate area detector in the Institute of Physics, Chinese Academy of Sciences (Beijing, China). Before data collection, the crystals were flash frozen in liquid N_2 after being immersed in Paratone-N oil, used as a cryoprotectant. The data were processed with the HKL suite of programs (32) and Raxis data processing software.

The three complex structures were solved by molecular replacement using AMORE (33), and solutions were obtained using the unliganded structure (Protein Data Bank code 1LHP) as search model. After rigid body refinement, the $F_o - F_c$ maps showed clear electron density representing the three roscovitines. Models of the inhibitors were made using (*R*)-roscovitine from the CDK2/roscovitine crystal structure as the initial model. Parameter and topology files for the three roscovitines were made using XPLO2D (Uppsala Software Factory). Crystallography and NMR System software (34) was used for refinement of coordinates and *B*-factors. Final models were obtained after several cycles of positional refinement and manual rebuilding using program O (35), and addition of water molecules. The quality of the final structures was verified using PROCHECK (36). The Ramachandran plot for the three inhibitors showed that the three structures had good stereochemistry. Structural statistics are shown in Table I. Coordinates and structure factors have been deposited in the Protein Data Bank (codes 1YGK, 1YGJ, and 1YHJ) (Table I).

RESULTS AND DISCUSSION

Crystal Structure of PDXK·Roscovitine Complex: Roscovitine Binds in the Pyridoxal Binding Site—We were able to obtain crystals of PDXK in complex with (*R*)-roscovitine at pH 8.2. Similar to the PDXK/AMP-PCP/pyridoxamine crystal, the PDXK·(*R*)-roscovitine complex structure belongs to the $P3_121$ space group, with the complex having one monomer in the asymmetric unit. The overall structure of PDXK contains 9 α-helices, 10 β-strands, and 3 segments of 3_{10} helices. The 10 β-strands form a central β-sheet flanked by α2, α3, α4, α5, and α6 on one side and α1, α7, α8, and α9 on the other side (Fig. 1*A*). (*R*)-Roscovitine binds in the groove formed by the ends of β-strands on the enzyme surface. The electron density for all atoms of the inhibitor (*R*)-roscovitine (and the two related purines, see below) was clear and strong (Fig. 1*B*). Surprisingly, (*R*)-roscovitine, as well as its inactive analogs, binds in the pyridoxal-binding site rather than at the ATP-binding site as initially expected (Figs. 1*A* and 2A). In the PDXK·(*R*)-roscovitine complex, PDXK interactions with (*R*)-roscovitine are characterized by predominantly hydrophobic and van der Waals interactions and hydrogen bonds (Fig. 2*B*). The purine ring of roscovitine is enclosed in a hydrophobic pocket formed by Tyr^{84}, Val^{19}, Val^{115}, and Gly^{232}. The benzyl ring has hydrophobic interactions with Val^{41} and Arg^{86}. Three direct hydrogen bonds are formed between (*R*)-roscovitine and the surrounding amino acid residues. One bond is formed between N^7 of (*R*)-roscovitine and the hydroxyl group of the Ser^{12} side chain. The second bond is formed between N^1 of (*R*)-roscovitine and the hydroxyl group of Thr^{47}. The third bond is formed between N2B of (*R*)-roscovitine and the same Thr-47 hydroxyl group. In contrast, in the PDXK·AMP-PCP·pyridoxamine complex, PDXK interacts with pyridoxamine thorough three hydrogen bonds formed between the N^1, O^3, and O^5 atoms of pyridoxamine and the side chains of Ser^{12}, Thr^{47}, and Asp^{235} of PDXK, respectively.

Comparison of the roscovitine-binding site in the CDK·roscovitine complexes (21, 26) and in the PDXK·(*R*)-roscovitine complex revealed that the atoms of roscovitine involved

TABLE I
Structure determination and refinement of PDXK in complex with (R)-roscovitine, N^6-methyl-(R)-roscovitine (2), and O^6-(R)-roscovitine (4)

	PDXK/(*R*)-roscovitine	PDXK/N^6-methyl-(*R*)-roscovitine	PDXK/O^6-(*R*)-roscovitine
Protein Data Bank file	1YGK	1YGJ	1YHJ
Data collection statistics			
Space group	$P3_121$	$P3_121$	$P3_121$
Cell dimension(Å)	$a = b = 102.8$, $c = 58.6$	$a = b = 100.9$, $c = 55.7$	$a = b = 103.2$, $c = 58.5$
Resolution (Å)	2.6	2.7	2.8
Unique reflections	10,910	9,190	9,065
Completeness, %	99.0 (99.3)	99.6 (99.1)	99.6 (100)
R_{merge} [a,b]	0.047 (0.353)	0.087 (0.314)	0.105 (0.267)
Refinement statistics			
R_{work} [b]	23.48	21.68	22.56
R_{free} [c]	27.08	27.98	28.51
Root mean square deviation from ideal geometry of final models			
Root mean square deviation bonds (Å)	0.015	0.015	0.012
Root mean square deviation angles (°)	2.38	1.71	2.03
Average B-factor (Å^2)			
Protein atoms	42.9	39.9	42.9
Ramachandran			
Most favored	78.8%	86.1%	79.4%
Additional allowed	18.2%	13.5%	19.5%
Generously allowed	2.9%	0.4%	1.5%

[a] $R_{merge} = \Sigma_h\Sigma_i(|I_i(h) - \langle I(h)\rangle|)/\Sigma_h\Sigma_i\ I_i(h)$, where $I_i(h)$ is the ith integrated intensity of a given reflection and $I(h)$ is the weighted mean of all measurements of $I(h)$.
[b] $R_{work} = \Sigma_h||F(h)_o| - |F(h)_c||/\Sigma_h|\ F(h)_o|$ for the 90% of reflection data used in refinement.
[c] $R_{free} = \Sigma_h||F(h)_o| - |F(h)_c||/\Sigma_h|\Sigma_h|F(h)_o|$ for the 10% of reflection data excluded from refinement.

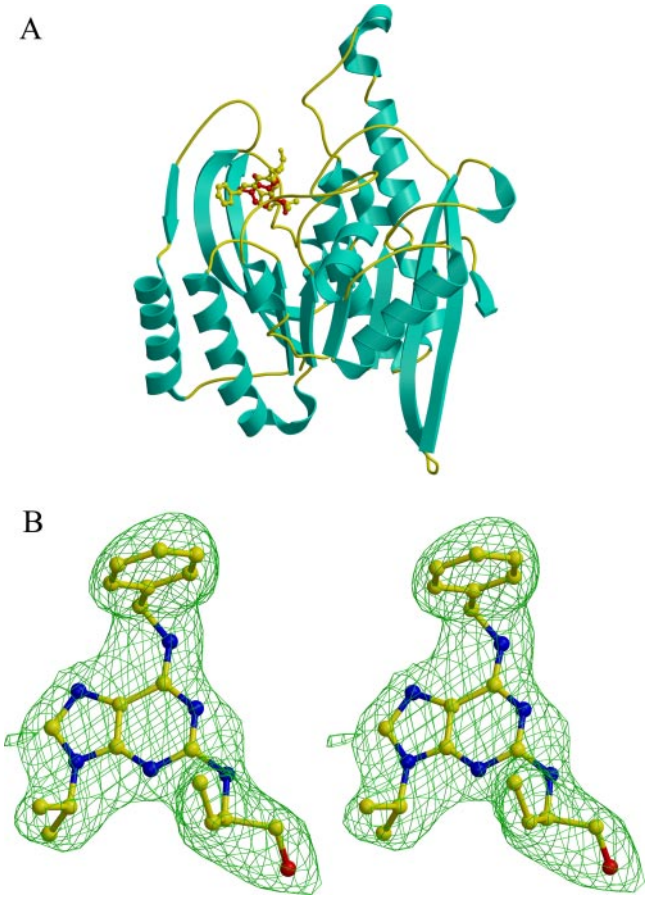

FIG. 1. **PDXK/(*R*)-roscovitine co-crystal structure.** *A*, a general ribbon view of PDXK showing the position of (*R*)-roscovitine (*yellow*) and that of pyridoxal (*red*). *B*, electron density of (*R*)-roscovitine co-crystallized with PDXK was calculated after rigid body refinement. The map (contoured at 1.0 σ level) was generated using MOLSCRIPT (38) and Raster3D (39).

in the interactions with each target are not the same (Fig. 2, *C* and *D*). In the CDK2·roscovitine (21) complex, the purine ring binds in the ATP-binding pocket. Leu^{83} interacts with roscovitine through two hydrogen bonds, involving N^7 and N^6 of the purine. In addition, a third weak hydrogen bond is formed between O^1 of the purine and a water molecule. Ile^{10} and Leu^{134} have hydrophobic interactions with roscovitine from two sides. A very similar binding mode was described in the CDK5·roscovitine complex (26).

PDXK Interacts with N^6-Methyl-roscovitine, a Protein Kinase Inactive Derivative—Roscovitine interactions with CDKs and PDXK are thus quite different. In the PDXK·(*R*)-roscovitine complex, N^6 of roscovitine does not make any contribution to its binding in the active site, whereas in the CDK·roscovitine complex N^6 acts as a hydrogen donor in a hydrogen bond with Leu^{83} of CDK2 (21) or Cys^{83} of CDK5 (26).

The N^6 position acts as a H-bond donor that is essential for the inhibitor/protein kinase interaction. We therefore synthesized two roscovitine analogs with modifications designed so that the H-bonding possibility at N^6 would be prevented (Table II). Either methylation on N^6 or replacement of N^6 by an oxygen, leading, respectively, to N^6-methyl-(*R*)-roscovitine (**2**) and O^6-(*R*)-roscovitine (**4**), converted roscovitine to derivatives devoid of protein kinase inhibitory activity (Table II).

We next immobilized (*R*)-roscovitine, N^6-methyl-(*R*)-roscovitine or purvalanol on Sepharose beads. Porcine brain extracts were loaded on these matrices, and the bound proteins were analyzed by SDS-PAGE after extensive washing (Fig. 3). Silver staining and Western blotting revealed the expected ERK1, ERK2, PDXK, and CDK5 proteins that specifically bind to (*R*)-roscovitine-Sepharose. No PDXK was detectable on purvalanol beads. In contrast, ERK1, ERK2, nor CDK5 were found on N^6-methyl-(*R*)-roscovitine-Sepharose beads while PDXK was present. This direct approach thus confirmed that N^6-methyl-(*R*)-roscovitine has lost the capacity to interact with its protein kinase targets, whereas its ability to interact with PDXK remains intact. Interaction of these two protein kinase inactive compounds with PDXK were further confirmed by the co-crystallization experiments (Fig. 4).

Crystallization of PDXK-selective Roscovitine Analogs with PDXK—The crystal of the PDXK·N^6-methyl-(*R*)-roscovitine complex was obtained at pH 8.2 and its structure was solved (Fig. 4, *A* and *C*). Superposition of the N^6-methyl-(*R*)-roscovitine and (*R*)-roscovitine complexes indicates that their overall

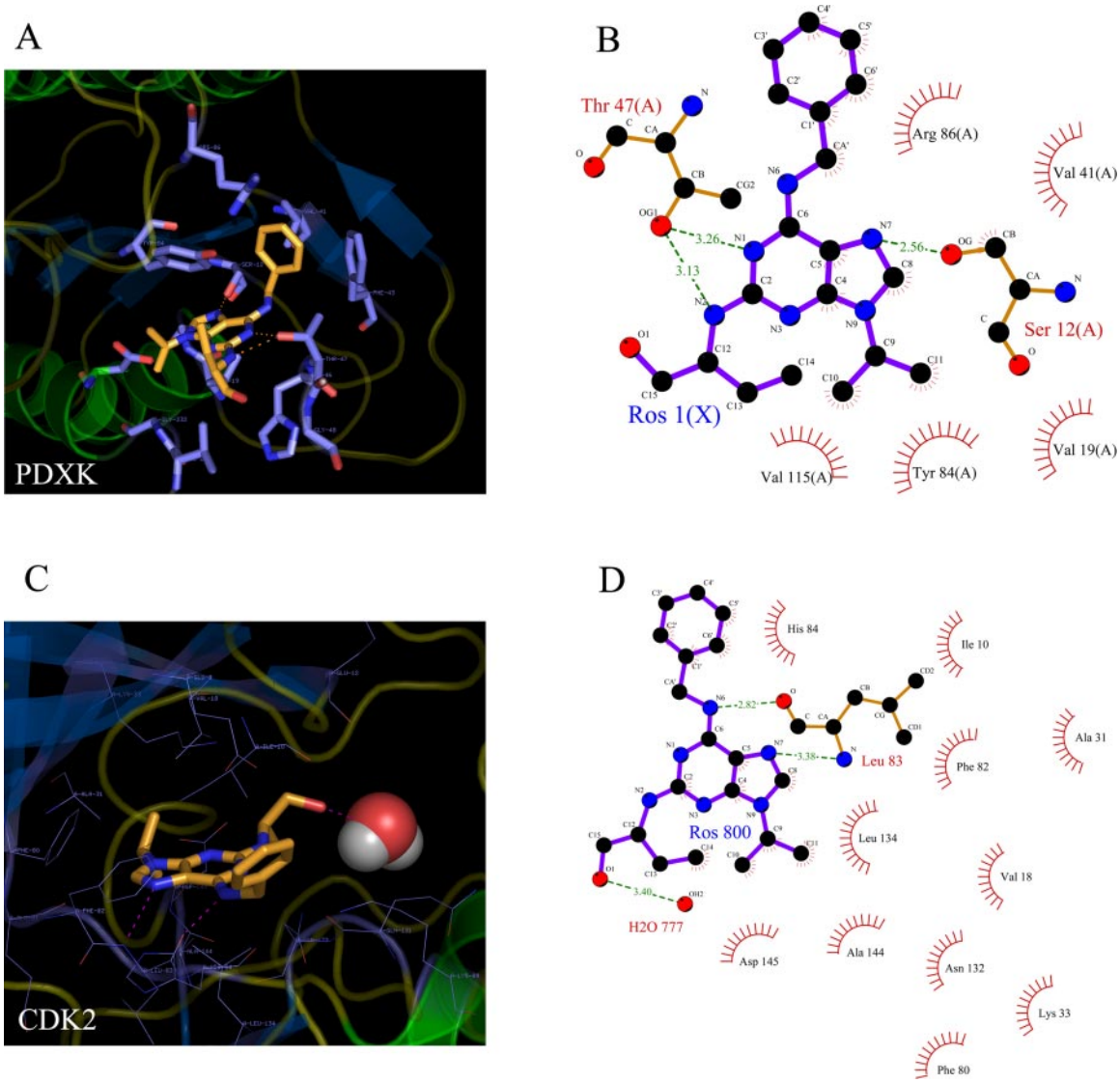

FIG. 2. **Interactions of (*R*)-roscovitine with PDXK (*A* and *B*) and CDK2 (*C* and *D*).** *A*, detailed stereo view of the pyridoxal-binding site of PDXK with bound (*R*)-roscovitine. The bound (*R*)-roscovitine molecule and its surrounding residues are shown as *stick models*. *B*, schematic atomic interaction map of (*R*)-roscovitine with PDXK amino acids. *C*, detailed stereo view of the ATP-binding site of CDK2 with bound (*R*)-roscovitine. The bound (*R*)-roscovitine is shown as a *stick model*, its surrounding residues are shown in *lines*, and the near water molecule is shown in *spheres*. *D*, schematic atomic interaction map of (*R*)-roscovitine with CDK2 amino acids and a water molecule. Figures were made using Pymol (www.pymol.org) and LIGPLOT (40).

structures are almost identical, that they form the same hydrogen bonds with PDXK (Fig. 5*A*), and that their binding in the pyridoxal-binding pocket involves very similar hydrophobic interactions. In the N^6-methyl-(*R*)-roscovitine·PDXK complex structure, the benzyl ring moved toward Phe^{43}, resulting in a slight conformational change of Trp^{52}, which is maintained in a position located adjacent to Phe^{43} (Fig. 5*A*).

Our initial attempts to obtain a PDXK/O^6-(*R*)-roscovitine crystal at pH 8.2 were unsuccessful. However, we obtained the PDXK·O^6-(*R*)-roscovitine complex crystal at pH 6.4 and determined its structure (Fig. 4, *B* and *D*). Previous studies indicate that the optimum pH for PDXK activity is ~6.5 (37), suggesting that this pH might provide a slight conformation change favorable for interaction with specific ligands. Comparison of PDXK in complex with O^6-(*R*)-roscovitine, (*R*)-roscovitine, and N^6-methyl-(*R*)-roscovitine indicates that they had a similar overall structure (Fig. 5*A*).

Comparison with PDXK in Complex with Other Ligands—Structural analysis of our previous PDXK·ATP (structure determined at pH 6.4) (7) and the PDXK·ADP·PLP (determined at pH 6.4) (8) complexes reveals that there is a 12-residue loop (117–128) connecting β5 and α4, which presents different conformations in the catalytic process carried out by PDXK (Fig. 6). There are two identical monomers (A and B) assembled by a non-crystallographic 2-fold axis in the asymmetric unit of PDXK/ATP. Loop 117–128 occupies a different position in monomers A and B. In monomer A the loop is restricted by the other symmetrical molecule in the crystal and occupies the pyridoxal binding pocket. This loop is referred to as "loop of state A." In monomer B, the loop is in contact with the solvent region of the crystal without any lattice limitation and completely sways to another direction, partially covering the ATP-binding site. This loop is then referred to as "loop of state B." PDXK can bind vitamin B_6 before ATP, suggesting that, under these conditions, this loop neither occupies the pyridoxal-binding site nor covers the ATP-binding site. In this situation the loop is referred to as "loop of state C." Based on this classification, loop 117–128 in the PDXK·O^6-(*R*)-roscovitine complex displays a loop of state C conformation in which PDXK contains roscovitine in the pyridoxal-binding site without ATP. Super-

TABLE II

Structure and kinase inhibitory properties of roscovitine and derivatives

Three purines were synthesized and tested on various kinases: (*R*)-roscovitine and the kinase inactive "N^6-methyl-(*R*)-roscovitine" (*R*-2-[6-(benzyl-methyl-amino)-9-isopropyl- 9*H*-purin-2-ylamino]-butan-I-ol) (**2**) and "O^6-(*R*)-roscovitine" (*R*-2-(6-benzyloxy-9-isopropyl-9*H*-purin-2-ylamino)-butan-1-ol) (**4**). IC_{50} values for several kinases are indicated under each structure. The purified protein kinases were assayed in the presence of 15 μM ATP and increasing concentrations of each purine. IC_{50} values, evaluated graphically, are in μM.

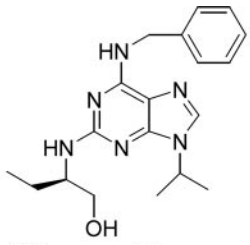

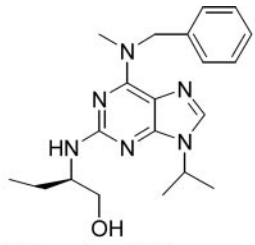

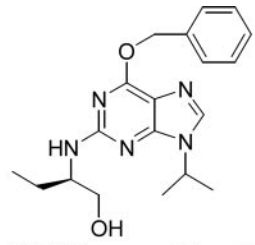

	(R)-roscovitine	N6-methyl-(R)-roscovitine (2)	O6-(R)-roscovitine (4)
CDK1/cyclin B	0.35	45	100
CDK2/cyclin E	0.40	250	250
CDK5/p25	0.20	45	200
Erk2	22	> 1000	700
CK1	100	> 1000	> 1000
DYRK1A	11	> 1000	250

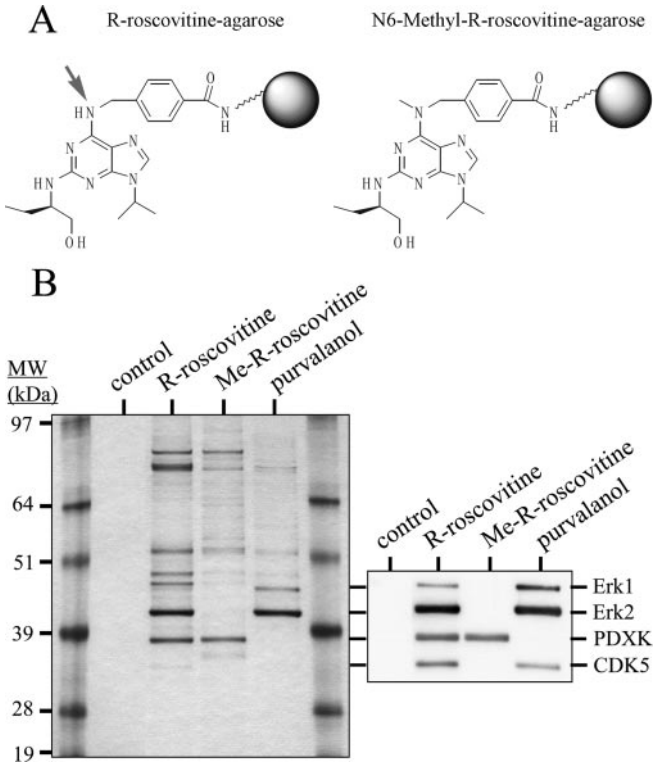

FIG. 3. **PDXK binds to immobilized N^6-methyl-(*R*)-roscovitine, an inactive derivative of roscovitine.** *A*, (*R*)-roscovitine and N^6-methyl-(*R*)-roscovitine were immobilized to agarose beads through a polyethylene glycol linker attached on the benzyl ring. A *arrow* indicates the N^6 position that provides an essential H bond between roscovitine and its CDK targets. *B*, a porcine brain extract was loaded on these beads, as well as control and purvalanol beads. Beads were extensively washed and the bound proteins were analyzed by SDS-PAGE followed by silver staining (*left*) and Western blotting (*right*) with antibodies directed against ERK1, ERK2, PDXK, and CDK5.

position of the PDXK·O^6-(*R*)-roscovitine and the PDXK·ATP complex structures shows that all main chain conformations are almost identical except for their 117–128 loops. In addition, the substrate binding pocket of the two complex structures are very similar, and no close contact was found between the ATP and O^6-(*R*)-roscovitine in the superimposed structures (Fig. 5*B*), which implies that the binding of O^6-(*R*)-roscovitine to PDXK does not perturb the ATP binding pocket. Interestingly, the loop of the PDXK·AMP-PCP·pyridoxamine complex (determined at pH 8.2 (8)) has been shown to be in line with the loop of state C of the PDXK·O^6-(*R*)-roscovitine complex. The difference between loop of state B and loop of state C is shown in Fig. 6. One notable difference is that in the PDXK·AMP-PCP·pyridoxamine complex, Tyr^{127} and Asp^{118} of the loop do not form hydrogen bonds with the β- and γ-phosphate group of ATP as observed in the PDXK·ATP complex structure. With the exception of the 117–128 loop, the overall structure of the monomeric PDXK·ATP complex is almost identical to the structures of the PDXK·(*R*)-roscovitine and the PDXK·AMP-PCP·pyridoxamine complexes. In addition, all three structures are in an "open/inactive" conformation, in contrast to PDXK/ADP/PLP (pH 6.4), which is in the "closed/active" conformation.

The conformation of PDXK·ADP·PLP complex is believed to be very close to the reaction transition state. Structural comparison reveals that the substrate binding pocket of PDXK·ADP·PLP is more compact than that of PDXK·O^6-(*R*)-roscovitine. Compared with PDXK·O^6-(*R*)-roscovitine, the loop connecting β2 and α2 in PDXK·ADP·PLP moved ~2 Å toward the substrate-binding site. Concurrently, the distance between two reaction group of substrates in PDXK·ADP·PLP is about 2 Å closer than that in PDXK·AMP-PCP·pyridoxamine (Fig. 6*B*).

Based on this analysis, the following conclusion can be reached. At the optimum pH (6.4), when PDXK only contains one substrate (ATP or pyridoxal), substrate binding does not induce any dramatic conformational change in PDXK (as observed, for example, in the PDXK·ATP and the PDXK·O^6-(*R*)-roscovitine structures). At pH 8.2, which is less favorable for enzyme activity, no conformational changes occur either when two substrates can bind simultaneously (as observed, for example, in the PDXK·AMP-PCP·pyridoxamine complex structure).

Asp^{235} is believed to be involved in initiating the phosphorylation reaction by abstracting a proton from the hydroxyl group of the vitamin substrate so that the hydroxyl oxygen atom can spontaneously attack the γ-phosphate of ATP. In the structure of PDXK/AMP-PCP/pyridoxamine (pH 8.2), Asp^{235} is forming a hydrogen bond (2.85 Å) with the $O^{5'}$ hydroxyl group of pyridoxamine. In contrast, a longer distance (3.4 Å) between Asp^{235} and the $O^{5'}$ atom of PLP is observed in PDXK/ADP/PLP

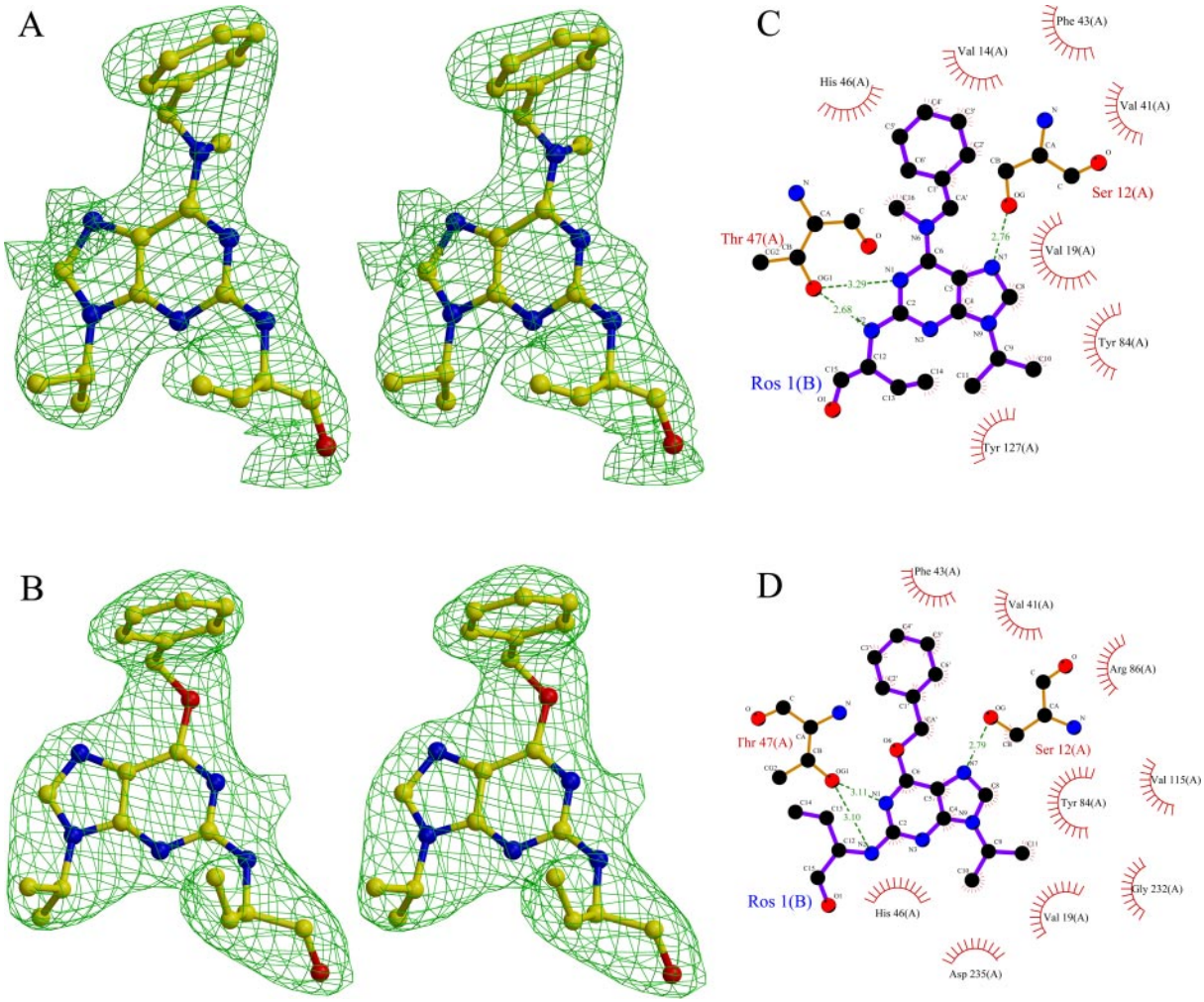

FIG. 4. **Interactions of N^6-methyl-(*R*)-roscovitine (2) and O^6-(*R*)-roscovitine (4) with PDXK.** *A* and *B*, electron densities of N^6-methyl-(*R*)-roscovitine (**2**) and O^6-(*R*)-roscovitine (**4**) co-crystallized with PDXK were calculated after rigid body refinement. The maps (contoured at 1.0 σ level) were generated using MOLSCRIPT (38) and Raster3D (39). *C*, schematic atomic interaction map of N^6-methyl-(*R*)-roscovitine (**2**) with PDXK amino acids. *D*, atomic interaction map of O^6-(*R*)-roscovitine (**4**) with PDXK amino acids.

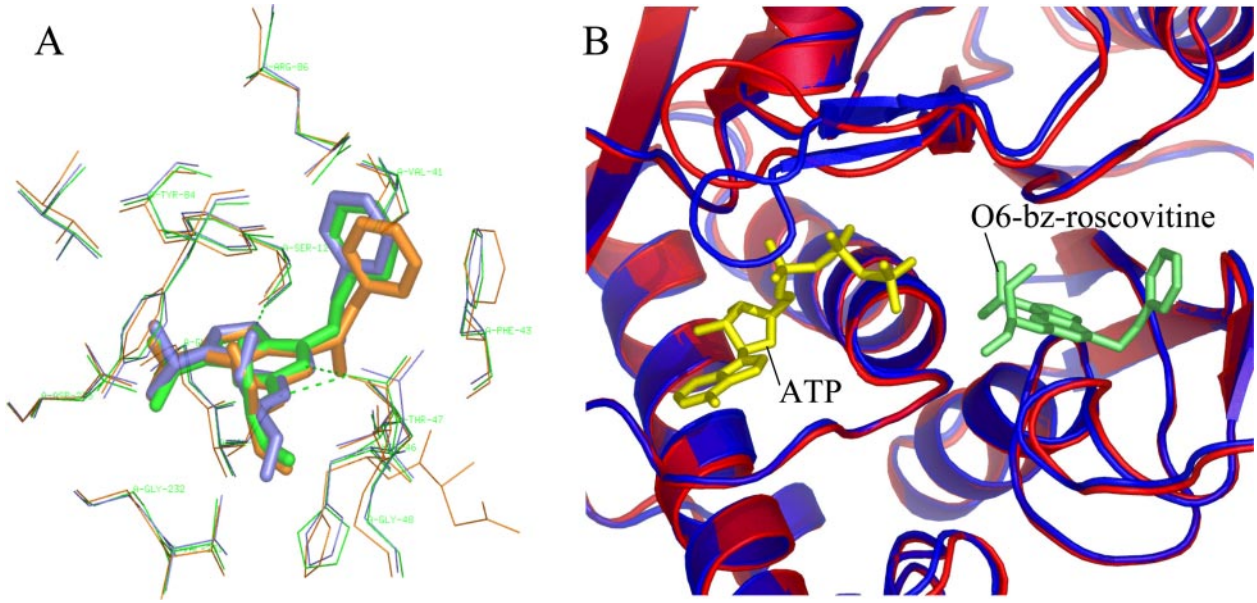

FIG. 5. *A*, superposition of (*R*)-roscovitine, N^6-methyl-(*R*)-roscovitine (**2**), and O^6-(*R*)-roscovitine (**4**) at the active site of PDXK. (*R*)-Roscovitine and the surrounding PDXK residues are shown in *green*, whereas N^6-methyl-(*R*)-roscovitine and O^6-(*R*)-roscovitine with the surrounding PDXK residues are shown in *orange* and *slate*, respectively. *B*, superposition of PDXK/O^6-(*R*)-roscovitine and PDXK/ATP. O^6-(*R*)-roscovitine is shown in *lime* and ATP in *yellow*. The backbone of PDXK/O^6-(*R*)-roscovitine and PDXK/ATP are shown in *red* and *blue*, respectively.

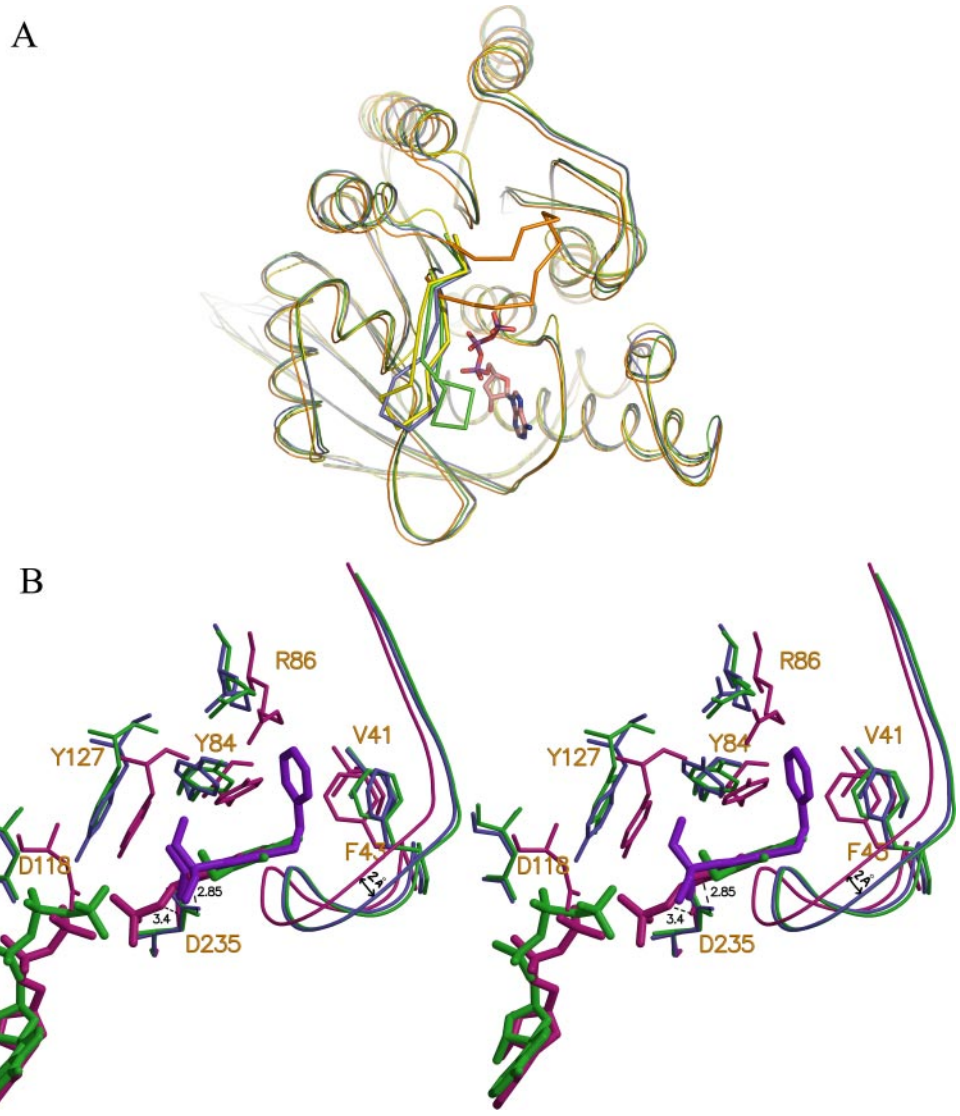

FIG. 6. **Superposition of PDXK in complex with various ligands.** *A*, superposition of PDXK/O^6-(*R*)-roscovitine and two monomers of PDXK·ATP complex reveal the loops have three different conformations. Loop of state A is *orange*, loop of state B is *green*, and loop of state C is *yellow*. The related loop of PDXK/AMP-PCP/pyridoxamine is lined with loop of state C and is shown in *slate*. *B*, superposition of PDXK/O^6-(*R*)-roscovitine, PDXK·AMP-PCP·pyridoxamine, and PDXK·ADP·PLP complexes reveals that the substrate binding pocket of PDXK·ADP·PLP is more compact than that in PDXK/O^6-(*R*)-roscovitine and PDXK/AMP-PCP/pyridoxamine. O^6-(*R*)-roscovitine is shown in *purple*, AMP-PCP and pyridoxamine are shown in *lime green*, PLP is shown in *violet red*, and ADP is shown in *violet red* also. In the PDXK·ADP·PLP complex the residues surrounding PLP and the loop connecting β2 and α2 are shown in *violet red*, in the PDXK·AMP-PCP·pyridoxamine complex the residues surrounding the pyridoxamine and the loop are shown in *lime green*, and in the PDXK/O^6-(*R*)-roscovitine complex the residues surrounding O^6-(*R*)-roscovitine and the loop are shown in *slate blue*.

(pH 6.4), indicating the protonation state of Asp^{235} (Fig. 6*B*). It is suggested that the protonation of Asp^{235} plays an important role in triggering the conformation switch on pH change, and the binding of substrates to the active site would induce further conformational change.

So far we have been unable to obtain any PDXK/ATP/roscovitine co-crystal structure, as if the two ligands were mutually exclusive. However, structural superimposition reveals that when O^6-(*R*)-roscovitine is modeled into the substrate binding pocket of PDXK/ADP/PLP, its benzyl ring will have close contacts with Arg^{86}, Phe^{43}, and Tyr^{127} (Fig. 6*B*). Therefore, it is reasonable to postulate that binding of ATP to PDXK/roscovitine may trigger a modest yet significant conformation change that influences the PDXK-roscovitine interaction. This hypothesis is substantiated by the "competing" effect of increasing concentrations of ATP on the binding of PDXK to immobilized roscovitine (22). Further studies will be required to understand this point fully.

In vivo, roscovitine may thus compete with pyridoxal binding to PDXK. However, the presence of ATP negatively influences the binding of roscovitine to PDXK, resulting in a very limited effect of roscovitine on PDXK catalytic activity. This effect of ATP might provide a safety mechanism for mammalian cells to prevent molecules other than vitamin B_6 from binding to the active site under the pre-reaction state, thus blocking their effects on PDXK. Our results revealed that the pyridoxal binding pocket has a surprising ability to accommodate large molecules such as roscovitine that are different from vitamin B_6, and roscovitine analogs with N^6 modifications show promise as specific inhibitors for PDXK.

Conclusion—This work constitutes the first report of a kinase inhibitor being crystallized with both its protein kinase targets (CDK2 and CDK5) and with a non-protein kinase, "off-target" enzyme (PDXK). Structural analysis reveals notable differences between the interactions of roscovitine with PDXK and CDK2/CDK5. Comparison of these structures

should allow us to design two different classes of roscovitine derivatives, the first one specifically targeting PDXK, whereas being devoid of inhibitory activity toward protein kinases, the second one specifically targeting protein kinases while no longer interacting with PDXK. N^6-Methyl-(*R*)-roscovitine (**2**) and O^6-(*R*)-roscovitine (**4**) represent two examples of the first class of PDXK-selective compounds. We are currently synthesizing roscovitine analogs belonging to the second class. The cellular effects and pharmacology of both classes of roscovitine analogs will be investigated in detail.

Acknowledgments—We are very grateful to Dr. Kirkness for providing the clone of human PDXK, Dr. J. Wang for the CDK5 and p25 clones, Dr. W. Becker for the DYRK1A clone, Dr. M. Cobb for ERK1/2, Dr. W. Harper for recombinant CDK2/cyclin E, O. Lozach for the CK1 assays, and K. Bettayeb for the CDK2/cyclin E assays.

REFERENCES

1. Kerry, J. A., Rohde, M., and Kwok, F. (1986) *Eur. J. Biochem.* **158,** 581–585
2. Percudani, R., and Peracchi, A. (2003) *EMBO Rep.* **4,** 850–854
3. Eliot, A. C., and Kirsch, J. F. (2004) *Annu. Rev. Biochem.* **73,** 383–415
4. Dakshinamurti, K., Paulose, C. S., Viswanathan, M., Siow, Y. L., Sharma, S. K., and Bolster, B. (1990) *Ann. N. Y. Acad. Sci.* **585,** 128–144
5. Laine-Cessac, P., Cailleux, A., and Allain, P. (1997) *Biochem. Pharmacol.* **54,** 863–870
6. Safo, M. K., Musayev, F. N., Hunt, S., di Salvo, M. L., Scarsdale, N., and Schirch, V. (2004) *J. Bacteriol.* **186,** 8074–8082
7. Li, M. H., Kwok, F., Chang, W. R., Lau, C. K., Zhang, J. P., Lo, S. C., Jiang, T., and Liang, D. C. (2002) *J. Biol. Chem.* **277,** 46385–46390
8. Li, M. H., Kwok, F., Chang, W. R., Liu, S. Q., Lo, S. C., Zhang, J. P., Jiang, T., and Liang, D. C. (2004) *J. Biol. Chem.* **279,** 17459–17465
9. Malumbres, M., Ortega, S., and Barbacid, M. (2000) *Biol. Chem.* **381,** 827–838
10. Harper, J. W., and Adams, P. D. (2001) *Chem. Rev.* **101,** 2511–2526
11. Malumbres, M., and Barbacid, M. (2001) *Nat. Rev. Cancer* **1,** 222–231
12. Monaco, E. A., 3rd, and Vallano, M. L. (2003) *Curr. Med. Chem.* **10,** 367–379
13. Vermeulen, K., Van Bockstaele, D. R., and Berneman, Z. N. (2003) *Cell Prolif.* **36,** 131–149
14. Cruz, J. C., and Tsai, L. H. (2004) *Trends Mol. Med.* **10,** 452–458
15. Smith, P. D., O'Hare, M. J., and Park, D. S. (2004) *Trends Mol. Med.* **10,** 445–451
16. Zhang, M., Li, J., Chakrabarty, P., Bu, B., and Vincent, I. (2004) *Am. J. Pathol.* **165,** 843–853
17. Wang, J., Liu, S. H., Fu, Y. P., Wang, J. H., and Lu, Y. M. (2003) *Nature Neurosci.* **6,** 1039–1047
18. Knockaert, M., Greengard, P., and Meijer, L. (2002) *Trends Pharmacol. Sci.* **23,** 417–425
19. Fischer, P. M., Endicott, J., and Meijer, L. (2003) in *Cell Cycle Regulators as Therapeutic Targets* (Meijer, L., Jézéquel, A., and Roberge, M., eds) Vol. 5**,** pp. 235–248, CNRS, Station Biologique de Roscoff, Roscoff, France
20. Meijer, L., and Raymond, E. (2003) *Acc. Chem. Res.* **36,** 417–425
21. Azevedo, W. F., Leclerc, S., Meijer, L., Havlicek, L., Strnad, M., and Kim, S. H. (1997) *Eur. J. Biochem.* **243,** 518–526
22. Wang, S., McClue, S. J., Ferguson, J. R., Hull, J. D., Stokes, S., Parsons, S., Westwood, R., and Fischer, P. M. (2001) *Tetrahedron Asymmetry* **12,** 2891–2894
23. Bach, S., Knockaert, M., Lozach, O., Reinhardt, J., Baratte, B., Schmitt, S., Coburn, S. P., Tang, L., Jiang, T., Liang, D. C., Galons, H., Dierick, J. F., Totzke, F., Schächtele, C., Lerman, A. S., Carnero, A., Wan, Y., Gray, N., and Meijer, L. (2005) *J. Biol. Chem.* **280,** 31208–31219
24. McClue, S. J., Blake, B., Clarke, R., Cowan, A., Cummings, L., Fischer, P. M., MacKenzie, M., Melville, J., Stewart, K., Wang, S., Zhelev, N., Zheleva, N., and Lane, D. P. (2002) *Int. J. Cancer* **102,** 463–468
25. De la Motte, S., and Gianella-Borradori, A. (2004) *Int. J. Clin. Pharmacol. Therapeut.* **42,** 232–239
26. Mapelli, M., Massimiliano, L., Crovace, C., Seeliger, M., Tsai, L. H., Meijer, L., and Musacchio, A. (2005) *J. Med. Chem.* **48,** 671–679
27. Meijer, L., Borgne, A., Mulner, O., Chong, J. P. J., Blow, J. J., Inagaki, N., Inagaki, M., Delcros, J. G., and Moulinoux, J.P. (1997) *Eur. J. Biochem.* **243,** 527–536
28. Fabian, M. A., Biggs, W. H., Treiber, D. K., Atteridge, C. E., Azimioara, M. D., Benedetti, M. G., Carter, T. A., Ciceri, P., Edeen, P. T., Floyd, M., Ford, J. M., Galvin, M., Gerlach, J. L., Grotzfeld, R. M., Herrgard, S., Insko, D. E., Insko, M. A., Lai, A. G., Lelias, J. M., Mehta, S. A., Milanov, Z. V., Velasco, A. M., Wodicka, L. M., Patel, H. K., Zarrinkar, P. P., and Lockhart, D. J. (2005) *Nat. Biotechnol.* **23,** 329–336
29. Chang, Y. T., Gray, N. G., Rosania, G. R., Sutherlin, D. P., Kwon, S., Norman, T. C., Sarohia, R., Leost, M., Meijer, L., and Schultz, P. G. (1999) *Chem. Biol.* **6,** 361–375
30. Rosania, G. R., Merlie, J., Jr., Gray, N., Chang, Y. T., Schultz, P. G., and Heald, R. (1999) *Proc. Natl. Acad. Sci. U. S. A.* **96,** 4797–4802
31. Knockaert, M., Gray, N., Damiens, E., Chang, Y. T., Grellier, P., Grant, K., Fergusson, D., Mottram, J., Soete, M., Dubremetz, J. F., LeRoch, K., Doerig, C., Schultz, P. G., and Meijer, L. (2000) *Chem. Biol.* **7,** 411–422
32. Otwinowski, Z. (1993) in *Oscillation Data Reduction Program* (Sawyer, L., Isaacs, N., and Bailey, S., eds) pp. 56—62, Science and Engineering Research Council/Daresbury Laboratory, Warrington, UK
33. Navaza, J., and Saludjian, P. (1997) *Methods Enzymol.* **276,** 581–594
34. Brunger, A. T., Adams, P. D., Clore, G. M., DeLano, W. L., Gros, P., Grosse-Kunstleve, R. W., Jiang, J-S., Kuszewski, J., Nilges, N., Pannu, N. S., Read, R. J., Rice, L. M., Simonson, T., and Warren, G. L. (1998) *Acta Crystallogr. Sect. D* **54,** 905–921
35. Jones, T. A., Zuo, J. Y., Cowan, S. W., and Kjeldgaard, M. (1991) *Acta Crystallogr. A* **47,** 110–119
36. Laskowski, R. A., MacArthur, M. W., Moss, D. S., and Thornton, J. M. (1993) *J. Appl. Crystallogr.* **26,** 283–291
37. McCormick, D. B., and Snell, E. E. (1959) *Proc. Natl. Acad. Sci. U. S. A.* **45,** 1371–1379
38. Kraulis, P. (1991) *J. Appl. Crystallogr.* **24,** 924–950
39. Merrit, E. A., and Murphy, M. E. P. (1994) *Acta Cryststallogr. D* **50,** 869–873
40. Wallace, A. C., Laskowski, R. A., and Thornton, J. M. (1995) *Protein Eng.* **8,** 127–134